




PEEK filament characteristics before and after extrusion within fused filament fabrication process

Cleiton André Comelli^{1,*} , Richard Davies¹, HenkJan van der Pol², and Oana Ghita¹

¹ College of Engineering, Mathematics and Physical Sciences, University of Exeter, Harrison Building, Streatham Campus, North Park Road, Exeter, UK

² Bond High Performance 3D Technology, Institutenweg 50, 7521 PK Enschede, The Netherlands

Received: 6 June 2021

Accepted: 16 October 2021

© The Author(s) 2021

ABSTRACT

The heating and extrusion process in fused filament fabrication (FFF) is significantly shorter than the conventional extrusion process where longer heating times and significant pressure are applied. For this reason, it is important to understand whether the crystal history of the feedstock is fully erased through the FFF process and whether the FFF process can be tailored further by engineering the crystallization of the feedstock filaments. In this context, a methodology for evaluating the influence of morphology and mechanical properties on different feedstock and extruded filaments is proposed. Filaments with three different PEEK 450G crystalline structures (standard crystallinity, drawn filament and amorphous filament) were selected and evaluated, before and after free extrusion. The resulting morphology, crystallinity and mechanical properties of the extruded filaments were compared against the feedstock properties. X-ray diffraction (XRD), transmission electron microscopy (TEM), differential and fast scanning calorimetry (DSC/FDSC) and tensile test were the techniques used to evaluate the materials. The results showed clear differences in the properties of the feedstock materials, while the analysis of the extruded filaments points to a homogenization of the resulting material producing mostly similar mechanical properties. However, the use of the drawn filament highlighted a statistically significant improvement in crystallinity and mechanical performance, especially in strain values. This conclusion suggests the innovative possibility of improving the quality of manufactured parts by tailoring the microstructure of the feedstock material used in the FFF process.

Handling Editor: Gregory Rutledge.

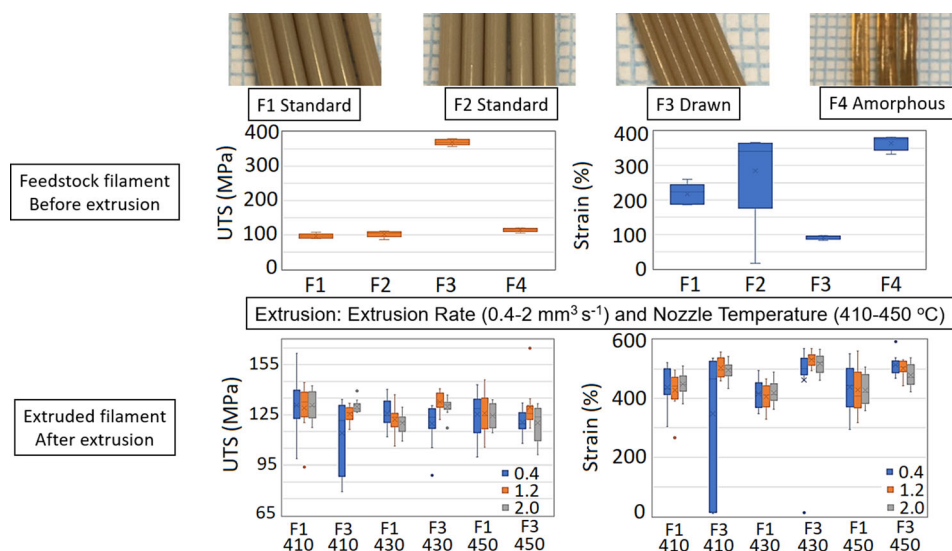
Address correspondence to E-mail: cc867@exeter.ac.uk

E-mail Addresses: richard.davies@exeter.ac.uk; hj.vanderpol@bond3d.com; o.ghita@exeter.ac.uk

<https://doi.org/10.1007/s10853-021-06652-0>

Published online: 03 January 2022

GRAPHICAL ABSTRACT



Introduction

Amongst additive manufacturing (AM) techniques, fused filament fabrication (FFF) is a simple, economic and popular process, usually chosen for several applications thanks to its hardware versatility, low cost, low material waste and the capacity of processing a reasonable range of thermoplastic materials [1–4]. Usually, the equipment is easy to maintain, uses stable feedstocks, and extensive options of open-source software and hardware are available [5, 6].

In FFF, the printing material goes through a dynamic thermal cycle, reaching the melting state inside the extruder nozzle (also known as liquefier), followed by a layered deposition process [7–9]. Usually, the extruder is mounted on an XY movable support and produces a filament in a pre-determined path on top of a build plate following a raster pattern and giving shape to successive layers [2, 10–12]. The molten filament experiences a quick solidifying process when in contact with the build plate or previous layers, and once the layer is complete, the build plate is lowered in the z-direction to produce a new layer, this process is repeated until the object is finally built [11–13].

Several processing parameters are adjustable, including feeding rate, nozzle temperature, and printing speed and, to obtain an optimal printing quality, an adequate parameter selection is necessary [1, 2, 13–18]. Performance levels also change according to the chosen polymer, which may present specific properties, such as different molecular weights, crystallinity levels, shape of the raw material, among others. These characteristics can affect performance during the FFF process with some studies showing such variations and their process influence among the same polymer grade, while in other cases, even the polymer colour may affect the performance [7, 19].

Moreover, a relatively wide variety of polymer types are available for FFF printers. Historically the most popular ones are poly(lactic acid) (PLA) and acrylonitrile butadiene styrene (ABS) [20–25]. More recently other options such as polyethylene terephthalate glycol (PETG), nylon, polycarbonate (PC), thermoplastic polyurethane (TPU—flexible), high-density polyethylene (HDPE), high-impact polystyrene (HIPS) were investigated [20, 22, 26–32].

To choose the right printing material, it is also necessary to take into account the part application. While simple prototype models can be easily printed with popular polymers, such as PLA, more serious

applications may require higher-performance polymers [26]. Poly (aryl ether ketones) (PAEKs) form a well-known polymer family based on high mechanical and chemical resistance, with wide use in harsh and demanding applications. PAEKs can also be found in filament form, and their application on FFF has already been investigated by some researchers [17, 18, 33–37].

PEEK 450G is part of the PAEK family and is resistant to hydrolysis, presenting low flammability, smoke, and toxicity levels at temperatures up to 240 °C, being one of the few polymers considered for metal replacement in some specific high-temperature applications [36]. PEEK can be used as a feedstock for FFF and depending on the production process, can present extensive variations in the microstructure morphology, which may influence its mechanical properties [38]. However, the majority of the available work concentrates on what happens during printing or at the end of the process, focused on parts/property performance, with less concern about the importance of feedstock filament quality and how it can influence the process.

One of the main reasons for the initial polymer microstructure to have a significant influence on the process is the melt-memory, a phenomenon that can affect the recrystallization of a polymer depending on the nature of its molten state [39]. For relatively low melting temperatures or short melting times, any remaining crystalline domains within a melted structure can act as self-nucleating agents of the new crystalline structure, and therefore affect the resulting semicrystalline microstructure [40–42]. Since the melting time is relatively fast in the FFF process, with temperatures that can vary according to the equipment characteristics and processing parameters used, a close evaluation of the melting mechanism is important to better understand the resulting microstructure.

Moreover, significant modelling has been done on the temperature profile during the layer-to-layer deposition, usually assuming that the polymer has no crystal history at the nozzle exit point [2, 43, 44]. However, this has not been confirmed in any study, and since the filaments are exposed to a fast-heating cycle, depending on the crystal structure and the level of polymeric chains alignment, it is unclear whether the crystal structure of the filament is fully erased.

In this context, the present work investigates the efficiency of the FFF process on melting PEEK 450G feedstocks with different crystallinity levels and polymeric chain alignment. The properties of the feedstock filaments and extruded filaments are compared before and after processing, discussing whether the crystal structure and mechanical properties of the feedstock filaments are fully lost throughout the extrusion process and whether the properties of the extruded filament could be influenced and controlled not only by the process but also by the properties of feedstock filament.

Materials and methods

Raw materials

Victrex PEEK 450G was used for this study, and the main characteristics of this material are presented in Table 1.

Four different feedstock filaments produced with PEEK 450G were selected:

- (1) PEEK 450G 1.75-mm filament supplied by Apium, referred to as F1;
- (2) PEEK 450G 1.75-mm filament supplied by Victrex referred to as F2;
- (3) Drawn PEEK 450G 1-mm filament supplied by Victrex referred to as F3;
- (4) Amorphous PEEK 450G 1/1.75 mm filament referred to as F4.

The amorphous feedstock filament was fabricated using a Delta extruder (model CTE-D16L640) to process Victrex PEEK 450G pellets. The PEEK pellets were first dried (5 h @ 120 °C). Right after the extrusion, the resulting filament was quenched in cold water to obtain amorphous PEEK filaments to be used as feedstock in the FFF process. The quenching process was aided by a custom-made pulley with the desired filament profile. The pulley helped to maintain the filament shape and also kept the filament in contact with a cold water flow; however, the resulting 1.75-mm amorphous filaments presented internal microbubbles from the quenching process, a problem that was solved by increasing the pulling rate within the extrusion process, which decreased the filament diameter to 1 mm. To avoid the presence of moisture or any effect of water uptake in the resulting filaments, a drying process similar to the one previously

Table 1 PEEK 450G main properties [45]

Property	Typical value
Tensile strength (MPa)	98
Tensile elongation (%)	45
Tensile modulus (GPa)	4
Melting point (°C)	343
Glass transition temperature T _g (°C)	143
Density (g cm ⁻³)	1.3
Drying temperature/time	150 °C/3 h or 120 °C/5 h (Residual moisture < 0.02%)

applied to the pellets was used. The average density for the filaments was around 1.3 g cm⁻³, with the only exception being the amorphous filament (F4), which presented a density of 1.02 g cm⁻³. All used feedstocks are shown in Fig. 1.

Fabrication of the extruded filament using the FFF process

It is well established that the printing process influences the performance of the parts [1, 3, 15, 28, 46, 47]. However, most of the research studies evaluate the performance at the final stage of the process by assessing the mechanical performance of the final component. At this stage, it is normally very difficult to ascertain the interactions between various process parameters and to understand how the printed material is influenced by the intrinsic properties of

the feedstock material. For this reason, a microstructural analysis of the feedstock material and extruded filaments obtained under different conditions was carried out using tensile test, transmission electron microscopy (TEM), X-ray diffraction (XRD), differential and fast scanning calorimetry (DSC/FDSC).

The feedstock filaments were extruded using a MendelMax 2 printer. The printer had an E3D style extruder and hot end, based on a single heating zone to melt the polymer. In the case of the 1 mm drawn and amorphous feedstock filaments, parts were machined to allow compatibility of the extruder with the filament's smaller diameter.

Extruded filaments were produced from feedstocks F1 and F3 only, since F2 proved to be statistically similar to F1 and the 1-mm amorphous filament (F4) was too soft, bending in the extruder mechanism and causing clogging problems.

The temperature and extrusion rate were varied during the experiment to verify the impact of these parameters on the produced filaments following a systematic approach based on a Design of Experiments (DoE). A factorial multilevel experiment allowed the investigation of the effect of each factor (nozzle temperature and extrusion rate) on the response variables (crystallinity and mechanical data).

Following this methodology, the combination of three different levels of temperature and extrusion rates resulted in nine different extrusion configurations (referred to as E1 to E9). The parameters used are summarized in Table 2.

Temperatures higher than 400 °C were used to guarantee a smooth extrusion process. The filaments were produced by free extrusion of the feedstock filaments into the air, in an environment with a temperature maintained at 20 °C. All specimens were

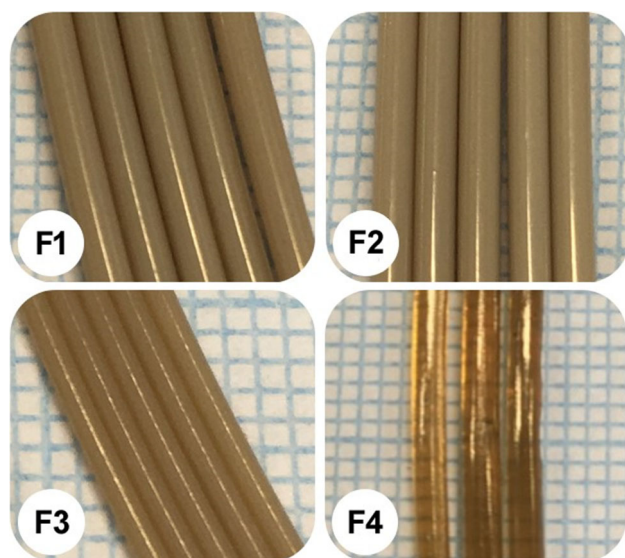


Figure 1 PEEK 450G feedstock filaments: F1—PEEK 450G; F2—PEEK 450G; F3—drawn PEEK 450G; F4—amorphous PEEK 450G filament.

Table 2 Feedstock extrusion factorial experiment configuration

Configuration	1	2	3	4	5	6	7	8	9
Extrusion rate ($\text{mm}^3 \text{s}^{-1}$)	0.4	1.2	2	0.4	1.2	2	0.4	1.2	2
Nozzle T ($^{\circ}\text{C}$)	410	410	410	430	430	430	450	450	450

produced with a nozzle output diameter of 0.6 and 400 mm of length.

These parameters were chosen because they are available in all types of FFF processes and are easy to vary. It is important to mention that parameters such as nozzle diameter or build room temperature also have an important influence; however, not all FFF equipment have a build room with temperature control. In addition, the 0.6 mm nozzle diameter was chosen as it presents a good ratio between productivity and finish quality in FFF processes. Other parameters that are also important, such as bed temperature, were not considered as the experiment was focused on analysing the filaments in a free extrusion approach, without interaction with substrates.

Although it can be argued that the extruded filament is not representative of the real process as it is extruded in air, extruding directly on the bed or on top of an additional layer was not a viable option as quality of the filament would be compromised due to the process of detaching of the individual extruded filaments from the bed or adjacent layer. Furthermore, as the interest was to accurately compare different feedstocks and check if the variation of FFF process parameters could influence the results, the free extrusion provided the solution with the least disturbance of the produced filaments.

Characterization techniques

Tensile test

Feedstocks were submitted to tensile test to understand the influence of crystallinity level and polymer chain alignment on mechanical properties.

The tensile test was initially performed on the feedstock materials, followed by the test on the free extruded filaments. The EZ20 Lloyds equipped with a 50-N load cell was used combined with Bollard style grips (Fig. 2), hence preventing the sliding of the specimens during the tensile test. All tests were repeated at least 5 times.

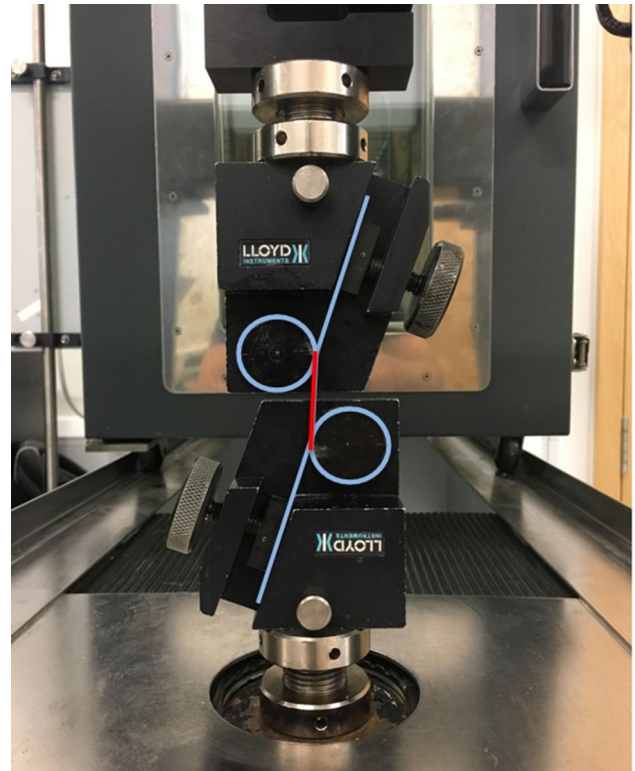


Figure 2 Tensile testing set up including the Bollard style grips and specimen fitting. The blue line defines the filament path within the rig with the red line highlighting the gauge length.

Due to the difference in samples diameters, before (1.75 mm) and after extrusion (0.6 mm), two test speeds were used: 50 mm min^{-1} for feedstock filaments and 300 mm min^{-1} for extruded filaments. This kept the test time to specimen fracture around 1 min for all specimens, following the time recommendations proposed by the ASTM D638 and ASTM D 3379. Since the comparison was made amongst the four feedstocks or amongst the extruded filaments, the different rates are not an issue. In order to determine the significance when comparing the mechanical results, a multiple comparison procedure was applied using Microsoft Excel.

DSC and Flash DSC

Feedstocks and extruded filaments were also submitted to DSC and Flash DSC experiments to determine the crystallinity and changes in crystal structure based on the filament residence time in the nozzle at various extrusion rates and temperatures.

For the thermal evaluation of the samples, a DSC 3 and a FDSC 2 + (Mettler Toledo, UK) were used. For the DSC, a standard heating and cooling cycle was applied across all feedstock filaments, at a heating and cooling rate of $10\text{ }^{\circ}\text{C min}^{-1}$ from 30 to $400\text{ }^{\circ}\text{C}$, under a constant nitrogen flow of 60 ml min^{-1} . All samples presented mass between 7 and 8 mg, and the melting enthalpy was measured using the reference heat of fusion of 130 J g^{-1} [48].

The majority of studies and models assume that the feedstock gets fully melted when passing through the nozzle [1, 7, 15, 49]. However, to date, there are no data confirming that this assumption applies to any crystal structure, or whether a drawn crystalline structure is likely to retain some of the original crystal history.

To better understand this phenomenon, a set of DSC and FDSC experiments were designed. Due to the fast-heating rate, the FDSC test is able to prevent the polymer reorganization that would take place in a standard DSC, and therefore replicate similar cooling and heating rates experienced by the material in the FFF process. An UFS1 type sensor with 16 thermocouples was used, and the sensor is able to achieve heating rates from 0.1 to $50,000\text{ }^{\circ}\text{C s}^{-1}$ and cooling rates from 0.1 to $4000\text{ }^{\circ}\text{C s}^{-1}$. Feedstock filament F1 (sample size of 260 ng) and F3 (sample size of 340 ng) were analysed, and the resulting data in combination with the mechanical results of the extruded filaments provided an insight into polymer behaviour at the exit point from the nozzle.

The first thermal cycle applied was a fast-heating cycle ($@1000\text{ }^{\circ}\text{C s}^{-1}$) (Fig. 3) to evaluate the F3 feedstock as received. The second experiment was focused on the standard feedstock F1, and the goal was to find a critical temperature and time that could melt the crystalline phase completely. In this case, the sample was fixed to the chip sensor using a slow heating cycle and a standard reference microstructure with crystallinity levels similar to the original feedstock (approximately 30%) was created using an isothermal crystallization process (300 s at $290\text{ }^{\circ}\text{C}$) (Fig. 4a). The temperature and time were defined

based on the PEEK 450G time–temperature–transformation chart [50]. This combination of time and temperature has been chosen for allowing a level of crystallinity similar to that originally found in feedstock 1.

Once the sample was attached to the sensor, the experiment proceeded with fast heating cycles to different target temperatures ($300\text{--}335\text{ }^{\circ}\text{C}$) and times (0,1 s; 5 s; 10 s) (Fig. 4b), always using as starting point the reference microstructure with 30% crystallinity. The last step was the evaluation of the remaining crystalline phase using a fast-heating cycle at $1000\text{ }^{\circ}\text{C s}^{-1}$ (see Fig. 4b).

The combination of temperature and time found capable of reducing the initial crystallinity by 50% was used in a third experiment for the feedstock F3, aiming to evaluate whether the drawn feedstock would maintain higher crystallinity levels when exposed to the same parameters. This thermal cycle was applied to the sample without it being previously fixed on the chip (which is done through a slow heating cycle), in order to avoid destroying the original aligned structure of the polymeric chains, characteristic of this feedstock. The same procedure was repeated for F1 to compare with the results previously obtained from the standard reference microstructure.

X-Ray diffraction (XRD)

The X-ray diffraction (XRD) analysis was carried out using a Bruker D8 advance diffractometer equipped with a copper anode at 40 mA and 30 kV. The measurements were taken with an angular range of $2\theta = 5\text{--}40^{\circ}$ with a step of $2\theta = 0.02^{\circ}$. The samples were prepared using small pieces of filaments to form a relatively flat surface, allowing the correct deflection of the X-rays. The resulting spectrum is formed from the constructive or destructive interferences stimulated by the interaction of the X-ray with the sample surface. For PEEK, typical peaks appear at angles $2\theta = 18.7^{\circ}$; 20.6° ; 22.8° ; and 28.8° , which correspond to the (110), (111), (200) and (211) planes, respectively [33, 51, 52]. The crystalline phase amount is calculated from the area of the sharp peaks A_c and the area of amorphous phase A_a , which is represented by the area of the curve bounded by the base of these peaks. The resulting crystallinity is given by Eq. (1):

Figure 3 FDSC thermal cycles of the feedstock filament F3.

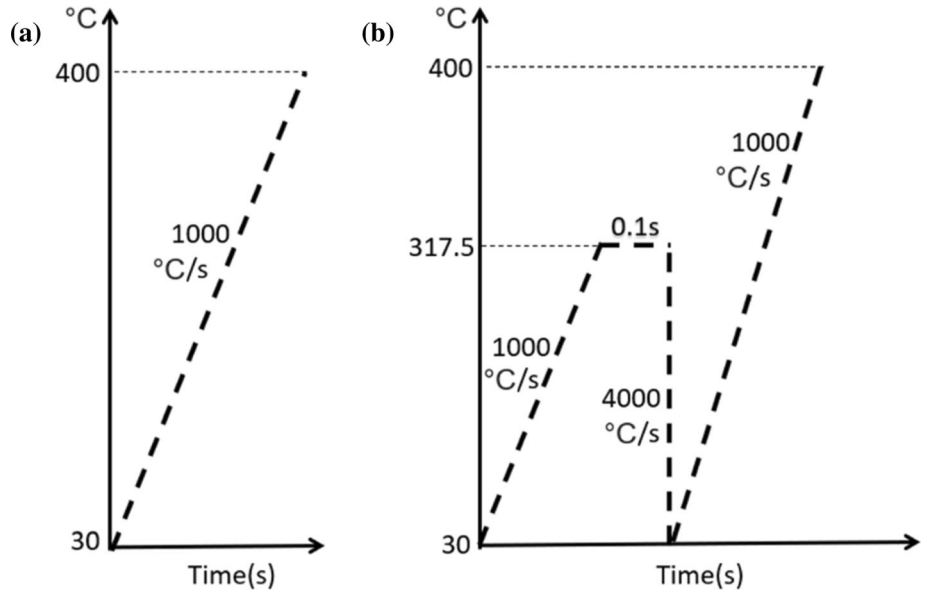


Figure 4 FDSC thermal cycles of the drawn filament feedstock F1.

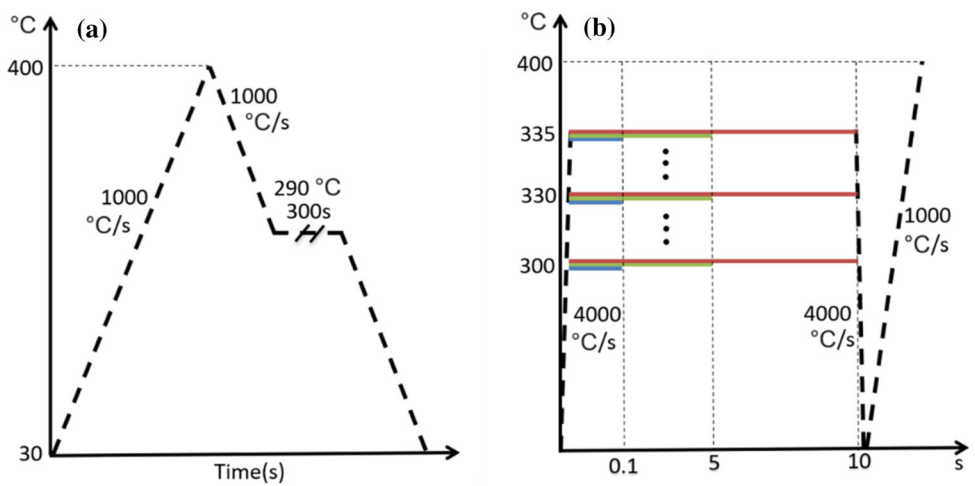
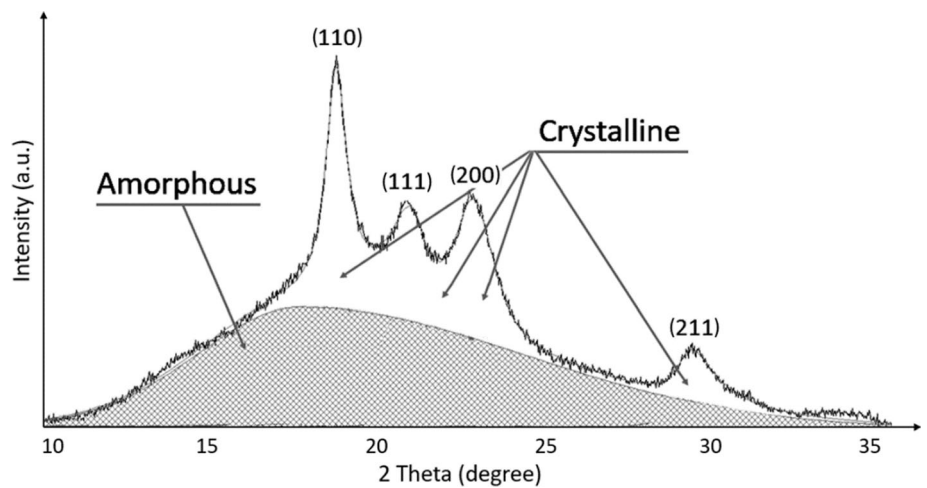


Figure 5 Typical XRD spectrum for PEEK (shaded region represents the amorphous phase, while peaks represent the crystalline phase).



$$X_c = \frac{A_c}{A_c + A_a} \quad (1)$$

The typical spectrum obtained for PEEK, with four crystalline peaks and a broad amorphous one, is shown in Fig. 5.

Transmission Electron Microscopy

Ultra-thin sections (around 70 nm) of the PEEK feedstocks F3 and F4 were prepared and placed on top of 100 mesh copper grids. A transmission electron microscope model JEOL JEM 1400 operated at 120 kV was used to obtain the images that were collected through a digital camera (ES 100 W CCD, Gatan, UK).

The evaluation of morphological aspects was accomplished through a qualitative visual analysis.

Results and discussion

Feedstock evaluation

The four feedstock filaments (F1–F4) were examined for their structural and mechanical properties. The experiments explored the feedstock behaviour based on three, very different crystallinities. F1 and F2 represent standard FFF feedstock filaments as provided by the majority of suppliers, F3 represents a highly aligned crystalline filament, and F4 is a fully amorphous filament. The amorphous feedstock filament (F4) was added to help understand the way the

overall microstructure influences the mechanical behaviour.

Mechanical properties of feedstock filaments

A typical stress–strain curve of each type of filament is shown in Fig. 6, and the summary for the feedstock mechanical test is presented in Table 3.

To determine which values were significantly different from each other, a multiple comparison procedure was applied using Microsoft Excel to obtain the P-value. The statistical analysis revealed that apart from F1 and F2, all other feedstocks presented significant differences for mean values. The strain values of F2 and F4 showed no significant difference, as shown in Table 4.

A box and whisker plot built with all measured stress and strain values also helps to evaluate the difference in performance for UTS and strain for all feedstocks, including mean and average values as well as standard deviation, as shown in Fig. 7.

The F3 drawn feedstock filament presented an incredible 369 MPa average stress with a Young's modulus of 1.9 GPa, while the amorphous filament F4 reached stress values in the similar region as F1 and F2 filaments, approximately 100 MPa, with a Young's modulus around 900 MPa.

It is possible to notice that the alignment of the polymer chains on the F3 filament eliminated the large strain range observed for the other tested feedstocks (Fig. 6), resulting in an uninterrupted increase in the stress values with the increase in the strain.

Figure 6 Typical stress x strain curves for feedstocks: F1—PEEK 450G; F2—PEEK 450G; F3—drawn PEEK 450G; F4—amorphous PEEK 450G filament.

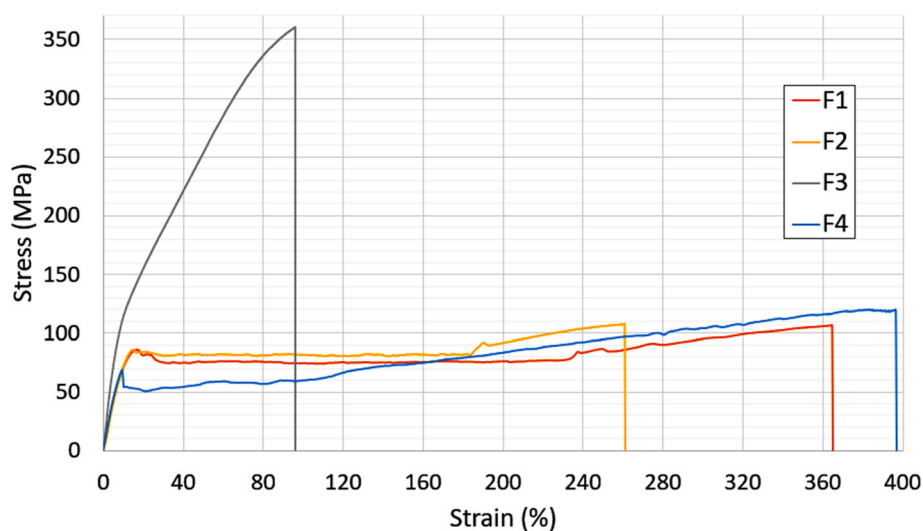


Table 3 Summary of feedstock mechanical test results: ultimate tensile strength (UTS) and strain

Feedstock	Number of repeat measurements	UTS (MPa)	SD	Strain (%)	SD	Young's Modulus (MPa)	SD
F1	5	96.25	7.30	217.69	30.79	960.4	11.0
F2	5	102.15	9.37	284.85	150.82	962.3	14.7
F3	10	369.60	7.97	91.22	5.51	1906.3	205.7
F4	5	115.05	5.67	364.95	20.63	998.1	141.6

Table 4 Multiple comparison procedure between means

UTS			Strain		
Group	P-value	Conclusion	Group	P-value	Conclusion
1.2	0.301	Not different	1.2	0.381	Not different
1.3	0.000	Different	1.3	0.001	Different
1.4	0.002	Different	1.4	0.000	Different
2.3	0.000	Different	2.3	0.045	Different
2.4	0.036	Different	2.4	0.302	Not different
3.4	0.000	Different	3.4	0.000	Different

When $P\text{-value} < 0.05$, the difference between the groups is significant ($\alpha > 95\%$)

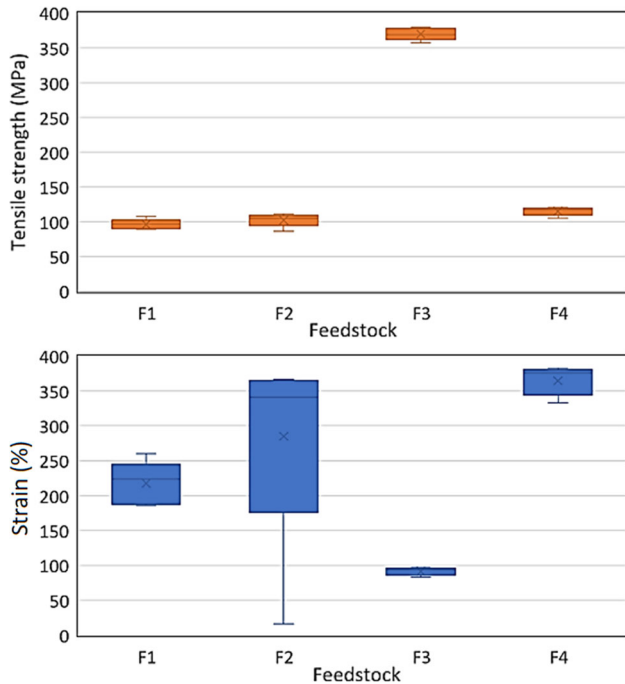


Figure 7 Box and whisker plot for feedstock filaments: stress and strain values.

Compensating for the changes in stress values, the strain of the drawn filament (F3) failed at approximately 91% as expected from a higher crystalline

structure where the amorphous F4 reached the highest strain value of approximately 400% with the F1 and F2 filaments varying significantly in values around 200 and 360%.

Such behaviour observed for the drawn filament is possibly related to the drastically reduced crystallographic slip or unfolding and stretching processes of the amorphous phase (Fig. 8) on the anisotropic highly aligned F3 feedstock [53]. Since most of the polymeric chains are strongly aligned in the axial direction of the filament, there is little deformation resulting in a more rigid filament, which presents greater mechanical resistance.

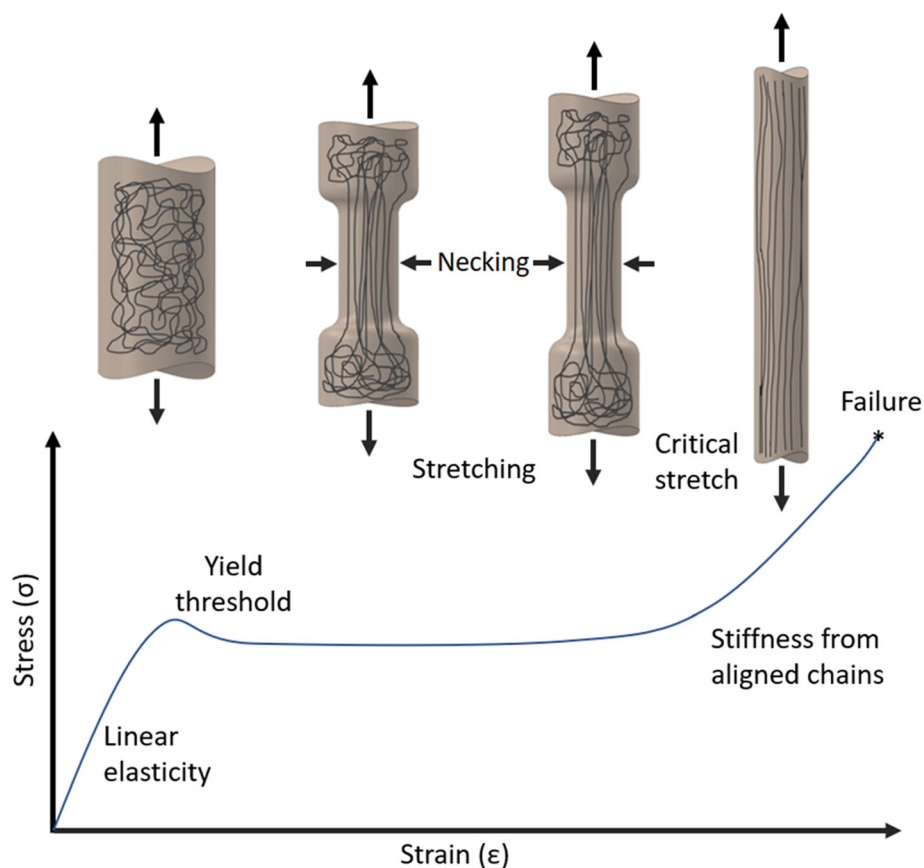
The stress–strain curve of the drawn filament F3 was very different in comparison with the other filaments. As the chains were already aligned along the filament axis during the drawing process, there was probably no considerably additional chain unfolding taking place during the test and the stress values increased constantly, without any additional necking. The yield point is not as evident, but it is possible to notice a variation on stress rate around 10% strain.

It was observed that F1 and F2 filaments started with an elastic deformation, reached the yield point, followed by a constant stress plastic deformation. In this region, a necking effect took place. Once the necking stretched across the entire gauge length, an increase in the stress was observed until the filament collapsed after reaching the highest stress. It is interesting to notice that the necking occurs in non-drawn crystalline filaments and in amorphous filaments as well, suggesting, in this case, a reorganization of the polymeric chains in the direction of traction instead of a crystalline structure unfolding [54, 55].

DSC & FDSC evaluation of feedstock filaments

To assess the thermal behaviour of the different feedstock filaments, each of them was subjected to a standard DSC analysis using the same basic thermal

Figure 8 Typical stress/strain polymer behaviour and polymer chain stretching mechanism.



cycle, as described in Sect. 2.3.2. The DSC thermograms for all feedstocks are shown in Figs. 9, 10, and 11.

Filaments F1 and F2 show standard profiles of semi-crystalline polymers melting and crystallizing. F4 shows the presence of a cold crystallization peak, a phenomenon normally observed in less crystallized polymers which reorganize themselves when passing the glass transition temperature [56, 57].

Feedstock F3 was expected to have a different thermal behaviour than F1 and F2. However, the resulting similarity of the thermograms and crystallinity values obtained from feedstocks F1, F2 and F3 during a standard DSC test was related to the reorganization of the polymer chains during the relatively slow heating promoted by the DSC during the melting cycle (Fig. 10a). This problem was addressed by using the FDSC with a heating rate of $1000\text{ }^{\circ}\text{C s}^{-1}$ (Fig. 10b), hence avoiding the reorganization of the polymer during the melting cycle due to the fast-heating rate.

The summary of all DSC results obtained from all feedstocks is shown in Table 5.

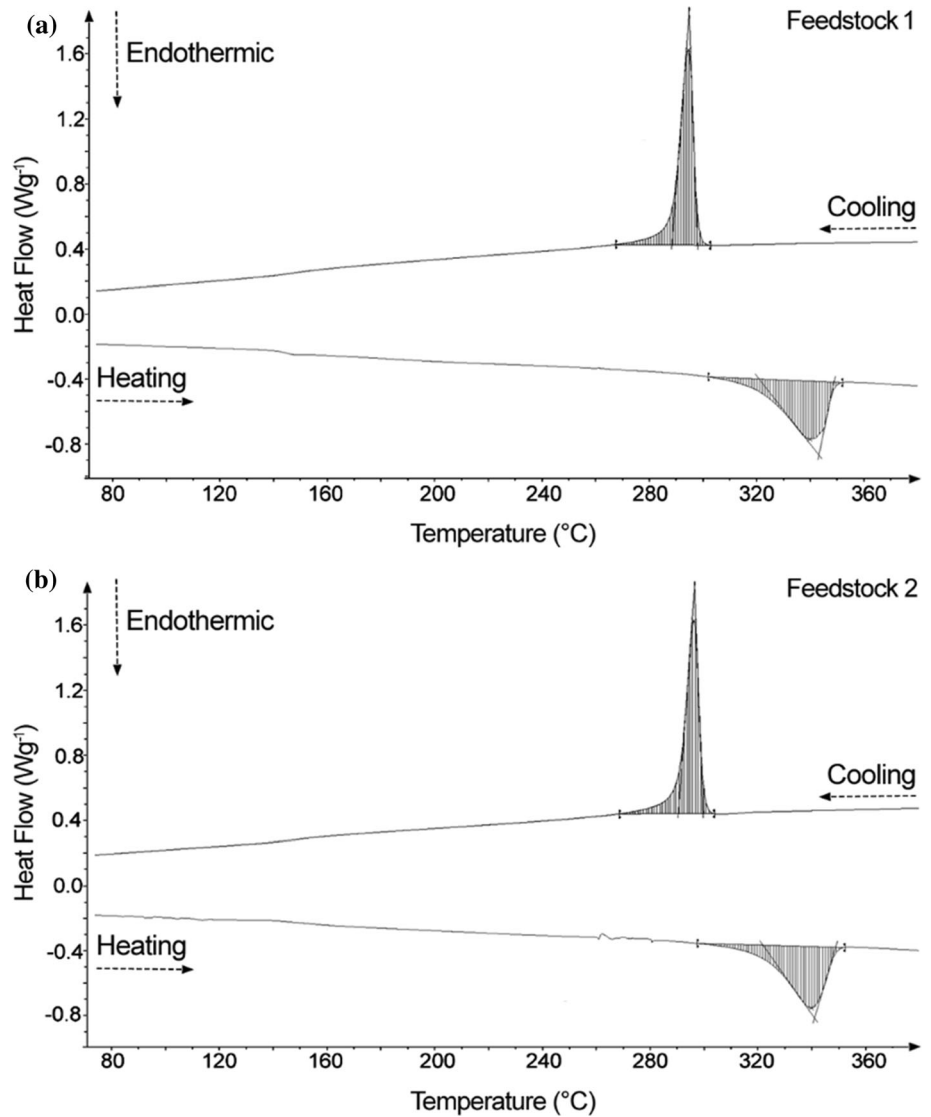
The highly aligned feedstock filament F3 reaches a crystallinity value of 40% in comparison with the standard F1 and F2 crystallinity values of approximately 30%; the glass transition interval also increased for the drawn filament samples.

Crystallinity evaluation of feedstocks using XRD analysis

The crystallinity values were also evaluated using XRD. For each feedstock, the main Bragg reflections of the orthorhombic unit cell of PEEK were detected at the angles 2θ of 18.82° , 20.80° , 22.78° and 28.82° , similar to previously reported in the literature [58, 59]. These peaks are associated with the diffraction planes (110), (111), (200) and (211), as shown in Fig. 12.

It can be noticed that the planes (110) and (111) of F3, drawn feedstock filament, presented considerably higher intensity when compared with peaks obtained for the standard filaments; as a consequence, the peak associated with the plane (111) was not clearly visible [60].

Figure 9 DSC curves for F1 (a) and F2 (b).



The curves were used for the degree of crystallinity calculations, and the resulting values are shown in Table 6.

The crystallinity values obtained from the XRD and the DSC are in agreement and follow similar trend, with the F3 filament having the highest percentage of crystallinity. The differences in crystallinity between the two methods are the result of the differences in the two techniques (surface over bulk measurement and thermal in comparison with optical method).

TEM analysis of feedstocks

The influence on the microstructure on the feedstock is examined in F3 and F4, as they represent the extremes of the crystallinity values according to the

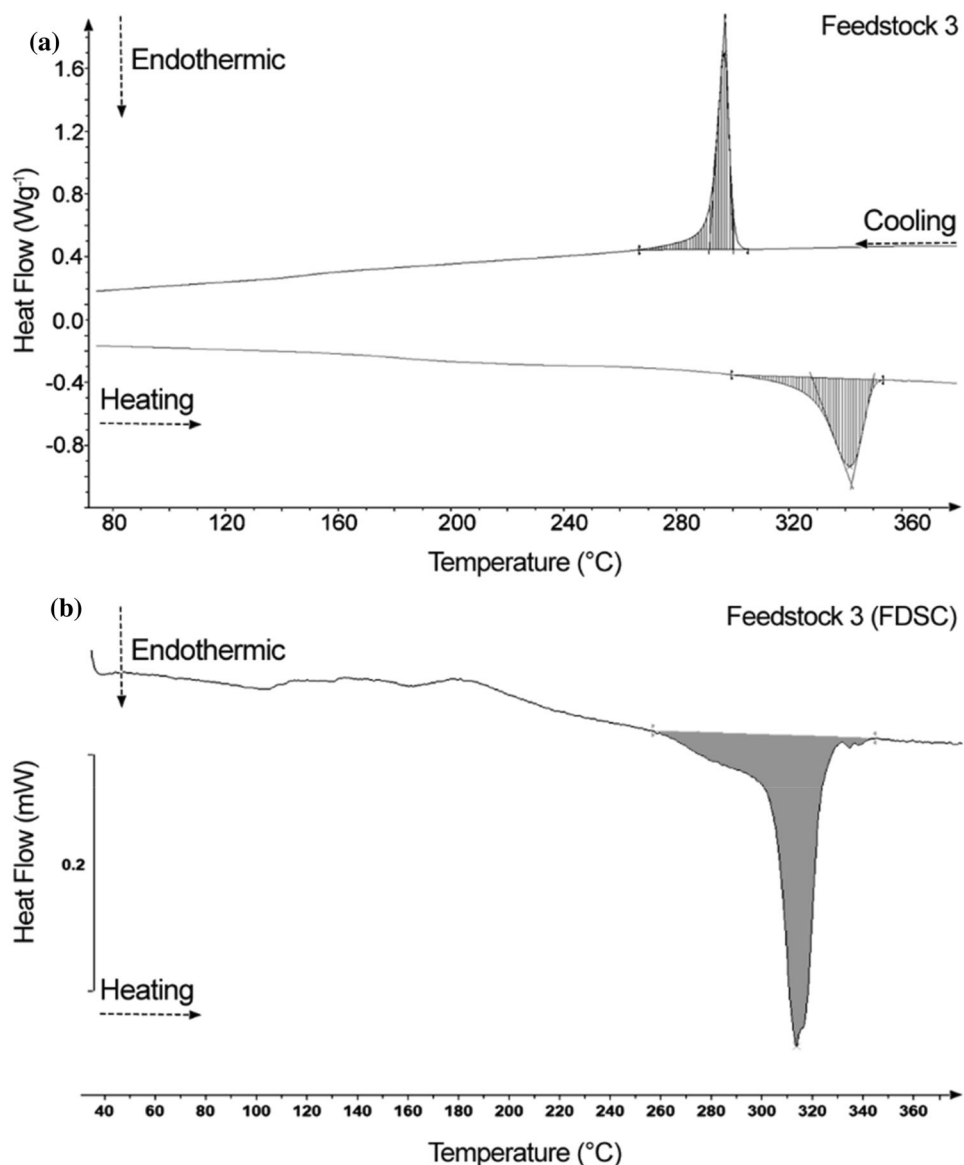
previous XRD analysis from Sect. 3.1.3. TEM images of the F3 and F4 filaments are shown in Fig. 13.

The image analysis showed two distinct structures of PEEK 450G (highlighted by the white circles); on crystalline PEEK samples, it is possible to identify crystallites of different sizes in a complex structure, and the polymer in the amorphous state presents smaller 2D crystal embryos from which possibly 3D crystals would normally develop. In this case, the crystallization has been suppressed through the quenching process.

Extruded filaments evaluation

The extruded filaments were subjected to mechanical testing. The average tensile strength and relative

Figure 10 DSC curves for F3 on DSC (a) and F3 on FDSC (b).



strain results of each extrusion configuration (for feedstocks F1 and F3) are presented in Table 7 along with the tensile modulus. The tensile curves for some representative samples are shown in Figs. 14 and 15. The mechanical results are also plotted in Figs. 16 and 17, and the multiple comparison analysis results are presented in Table 8. As explained in item 2.2, F4 was excluded from this experiment because it was not possible to extrude it, since it was too soft, flexing in the extruder mechanism and causing clogging.

The processing parameters did not significantly affect the mechanical properties of the extruded filaments, which presented similar results when comparing different extrusion temperatures and extrusion rates for the same feedstock. PEEK 450G is

a fast-crystallizing grade, as shown by crystallization kinetics of other studies [50]; therefore, any microstructure effects induced by the process parameters may be lost in a mechanical test under these conditions (free cooling in air) due to the fast-crystallizing nature of the polymer.

However, when comparing the performance obtained with the different types of filaments, it is possible to observe significant differences (Table 8), with the performance obtained for the filaments produced with F1 showing slightly smaller tensile strength than the filaments produced with F3—drawn filament (Fig. 16) for three process configurations. The significant differences between the groups

Figure 11 DSC curves for F4.

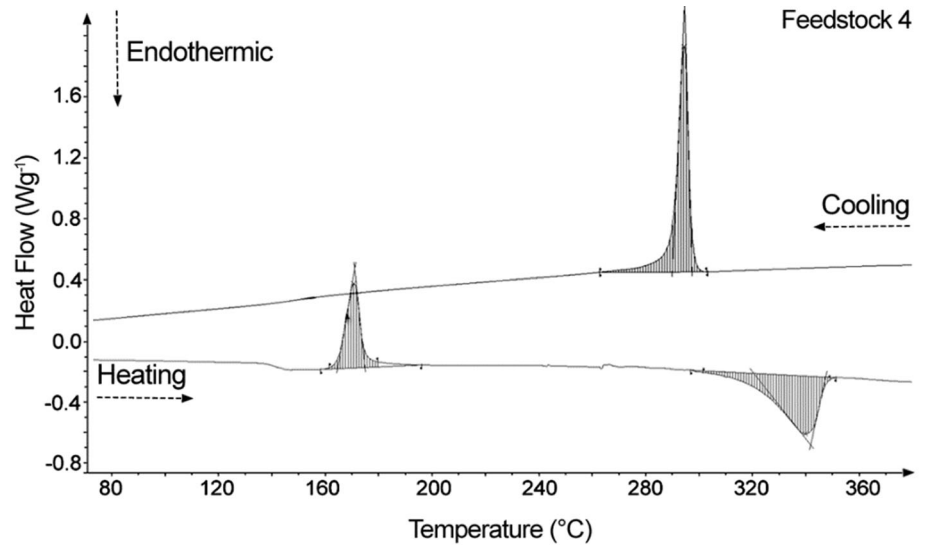
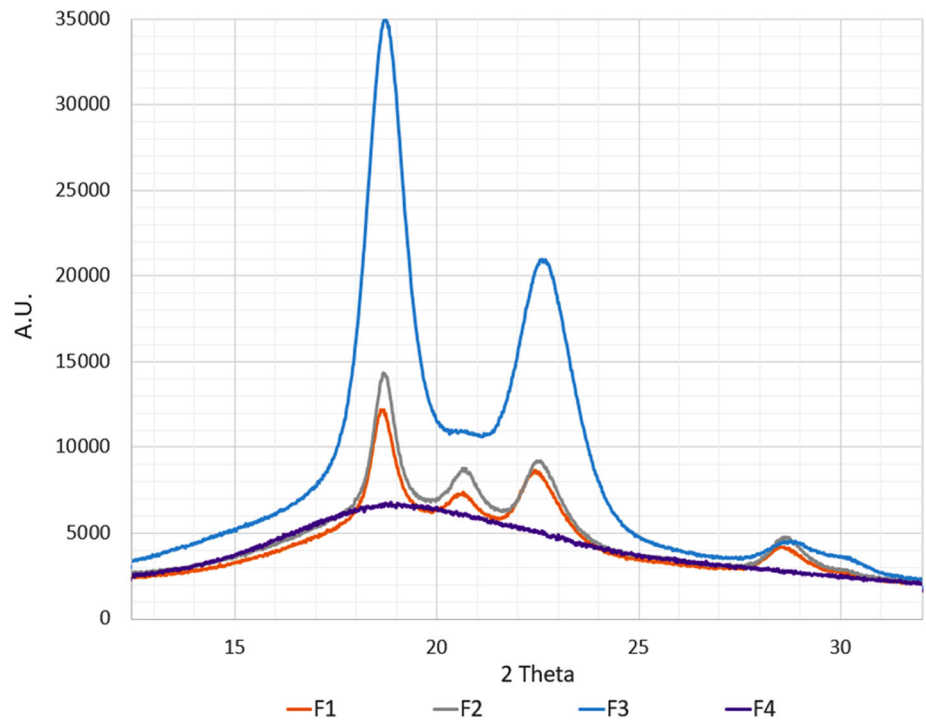


Table 5 DSC and FDSC results of feedstock filaments (F1, F2, F3 and F4)

Feedstock	F1	F2	F3	F4
Properties	Standard 1	Standard 2	Drawn	Amorphous
	1.75 mm	1.75 mm	1.00 mm	1.75 mm
Tm (°C)	339.84	339.78	341.52	339.85
Tg (°C)	145	147	160	142
Degree of crystallinity (%)	32.07	31.64	40.26	10.82
Tc (°C)	294.65	296.13	296.99	294.45
Tcc (°C) (cold crystallization)	–	–	–	170.65

Figure 12 XRD curves for all feedstocks.



could be linked with the presence of different crystalline structures.

The strain results also presented an interesting behaviour when comparing the F1 and F3 filaments, the drawn feedstock presented higher values when compared with the filaments from F1 (Fig. 17). Also, a different behaviour can be observed in the tensile test curves (Figs. 14 and 15) with the samples produced from F3 showing a larger plastic deformation region before presenting an increase in tension resulting in the sample breaking.

Table 6 Feedstock crystallinity levels

Sample	Crystallinity	
	%	SD
F1	33.10	0.61
F2	34.53	0.32
F3	44.57	0.55
F4	9.67	0.15

This may be an indication that the extruded filaments were affected by the initial microstructure features and that the original crystal structure was probably not entirely erased, with some memory effects [39, 41] playing an influence in the extruded filament, resulting in increased maximum strain.

Interestingly, the modulus seems to be influenced by the process, and the F1 extruded filament showed a slightly increase in modulus possibly due to some alignment effect induced by the change in diameter from 1.75 to 0.6 mm. The extruded filament F3, on the other hand, presented lower values and then its feedstock equivalent, possibly due to a smaller difference between the initial and final diameter from 1.0 to 0.6 mm. Also, a drawn filament is under tension during its fabrication which is not the case in the FFF extrusion process; therefore, a relaxation of the aligned polymeric chains is possible.

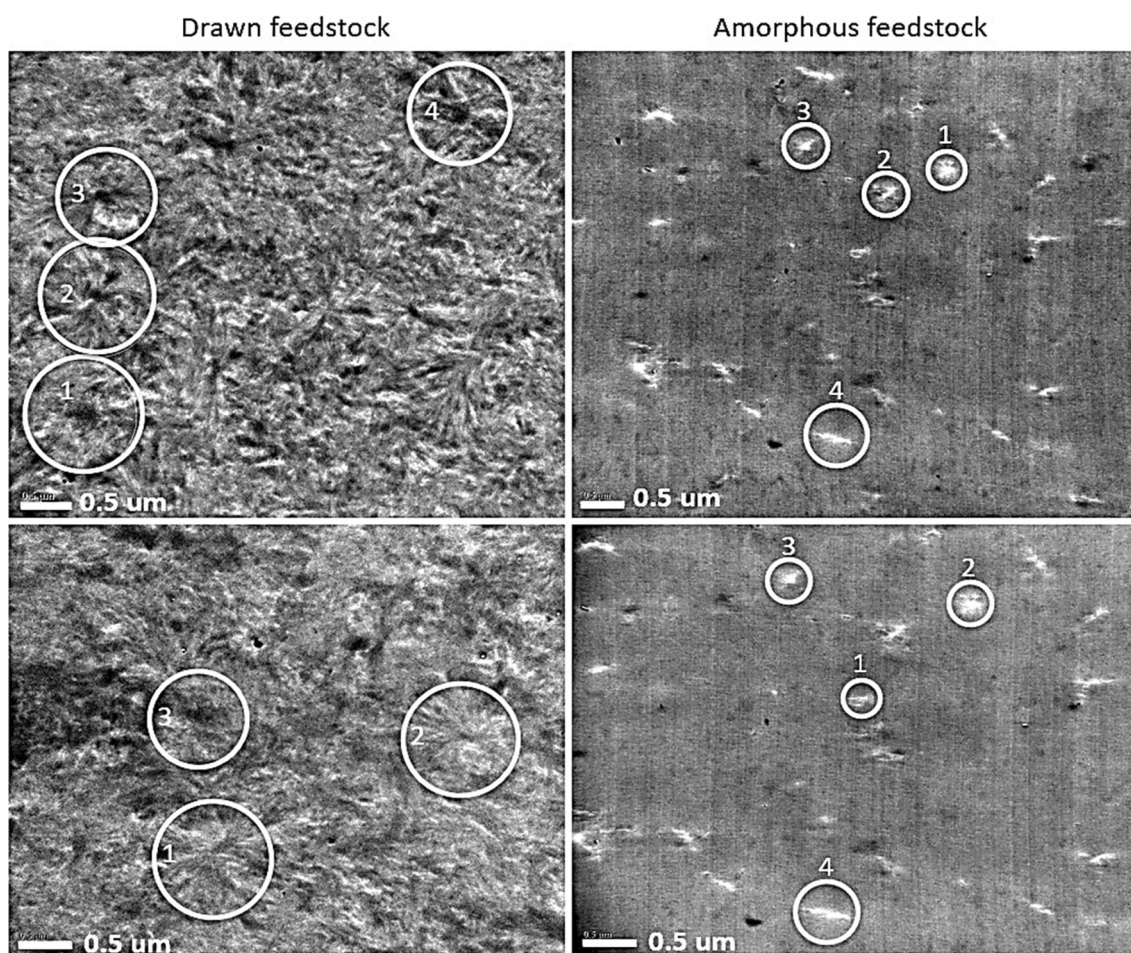
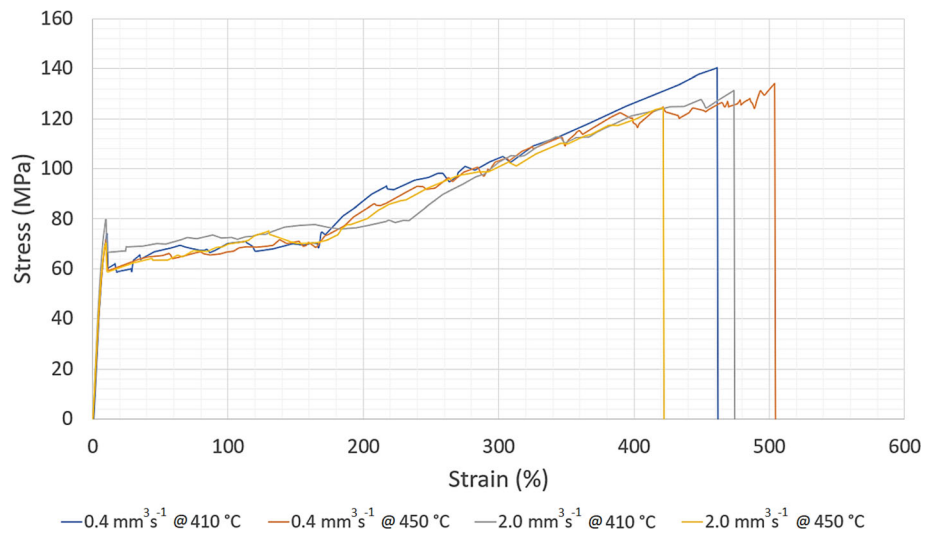


Figure 13 Microstructure of drawn crystalline feedstock (F3) and amorphous (F4).

Table 7 Average tensile strength and relative strain for extruded filaments

Feedstock	Ext. rate (mm ³ s ⁻¹)	Temp (°C)	UTS (MPa)	Strain (%)	Young's Modulus (MPa)
			Mean (SD) (10 repeats/set)	Mean (SD) (10 repeats/set)	Mean (SD) (10 repeats/set)
F1	0.4	410	130.75 (7.06)	453.93 (43.67)	1509.1 (293.4)
	1.2	410	133.03 (8.26)	445.99 (37.61)	1426.2 (264.8)
	2.0	410	130.70 (8.58)	449.63 (36.97)	1438.6 (212.6)
F1	0.4	430	125.90 (9.08)	417.20 (49.3)	1432.1 (215.2)
	1.2	430	122.24 (8.33)	406.75 (46.11)	1526.5 (261.3)
	2.0	430	120.16 (5.97)	419.11 (37.43)	1449.9 (218.6)
F1	0.4	450	128.30 (10.08)	454.07 (70.48)	1361.0 (287.6)
	1.2	450	126.96 (12.21)	428.88 (79.69)	1389.5 (202.5)
	2.0	450	124.60 (7.49)	428.79 (52.64)	1320.1 (186.0)
F3	0.4	410	126.57 (6.85)	348.41 (234.89)	1176.0 (49.4)
	1.2	410	125.52 (4.8)	505.39 (33.26)	1197.8 (87.6)
	2.0	410	129.87 (4.03)	496.71 (31.43)	1230.7 (59.3)
F3	0.4	430	123.19 (7.51)	513.18 (33.59)	1137.8 (50.8)
	1.2	430	132.81 (6.23)	533.07 (23.30)	1183.5 (47.5)
	2.0	430	130.00 (5.27)	519.12 (32.57)	1221.6 (93.3)
F3	0.4	450	120.62 (6.74)	514.12 (35.18)	1139.3 (27.6)
	1.2	450	129.45 (13.35)	502.12 (30.09)	1195.3 (117.4)
	2.0	450	120.17 (10.61)	479.69 (39.77)	1211.7 (73.2)

Figure 14 Stress x strain chart for extruded filaments F1.



XRD analysis of extruded filaments (F1 and F3)

The XRD crystallinity values for each tested extrusion configuration are shown in Tables 9 and 10.

As noticed throughout the mechanical results, the changes in extrusion conditions do not significantly affect the strength and strain of the filaments, based on the procedure used here for manufacture of the filament (extruded and cooled in air). Similarly, the crystallization is not affected by the changes in extrusion conditions. However, the overall XRD

crystallinity values for the extruded filament highlight some interesting features when comparing both filaments, with filaments produced with F3 showing higher crystallinity values when compared to filaments produced with F1, which could indicate an influence of the previous microstructure on increasing the resulting crystallinity.

As pointed out in earlier literature, sharper diffraction peaks can be correlated with greater crystallinity, which can be seen in Fig. 18 in which the drawn extruded filament (F3) maintains the

Figure 15 Stress x strain chart for extruded filaments F3.

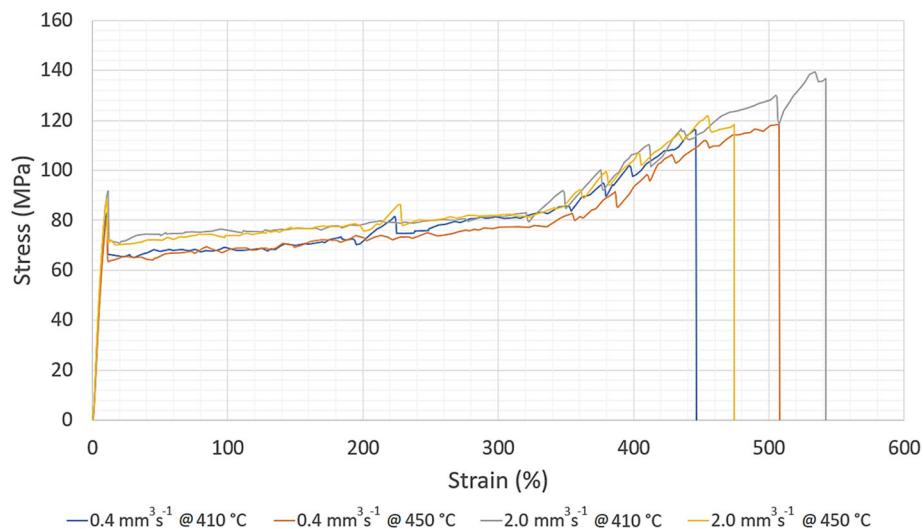
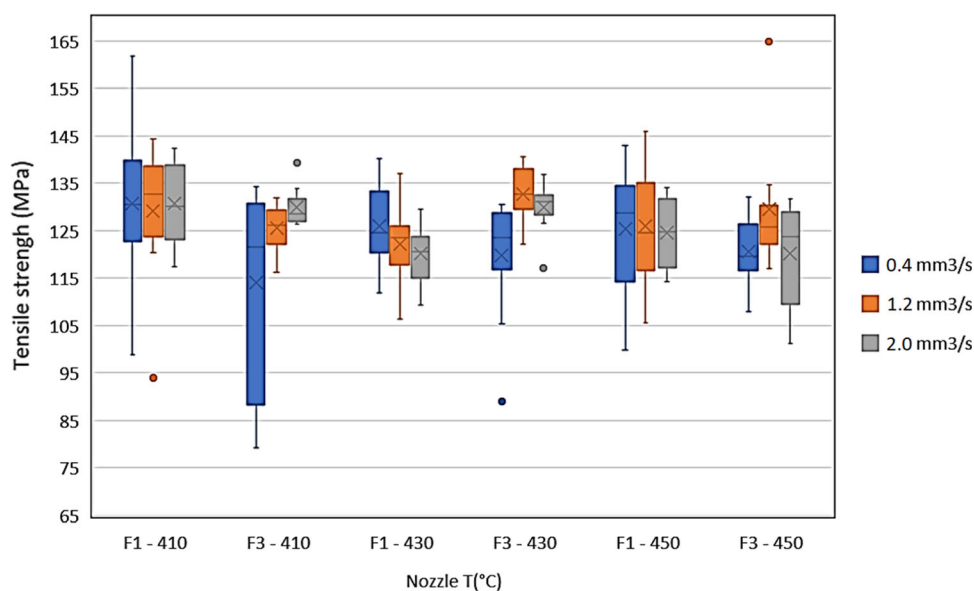


Figure 16 Average tensile strength for extruded filaments (F3-410 showed significantly larger scatter in the data).



highest crystallinity and shows sharper peaks [61]. This could be the result of changes in crystal morphology and crystal retention when being extruded.

Crystal remelt and crystal retention as a function of nozzle residence time and temperature

In order to determine the critical process temperatures and the residence times able to fully melt the crystal structure of the feedstock filament and whether there is any residual crystallinity left within the extruded filament, additional experiments were employed using the Flash DSC as explained in Sect. 2.3.2. The Flash DSC allowed to evaluate the

temperature and residence time influence using times ranging from 0.1 s to 5 s and 10 s and temperatures from 310 to 330 °C.

These times were chosen to provide longer and shorter residence times when compared with a standard FFF process. The temperatures were chosen in order to gradually approach the typical melting temperature of PEEK 450G (340 °C). After each isothermal cycle, the polymer was quickly cooled to 30 °C to generate a reference structure with 30% crystallinity (as explained in the experimental section) that would allow to compare the effect of each heating cycle subsequently tested.

After each cycle, residual crystallinity was measured based on the enthalpy of melting detected

Figure 17 Average strain for extruded filaments (F3–410 showed significantly larger scatter in the data).

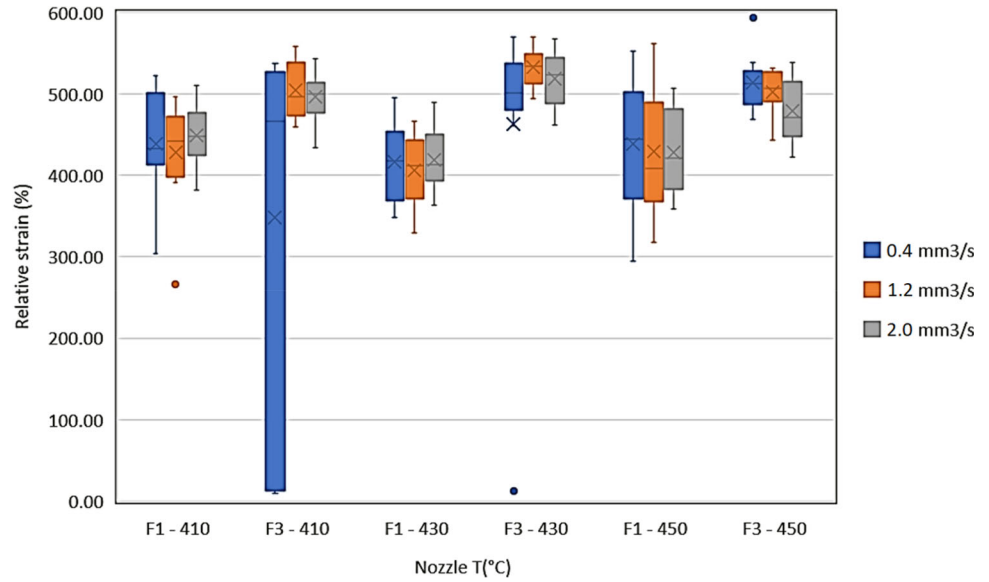


Table 8 Multiple comparison analysis results for tensile strength and strain between F1 and F3 (when P -value < 0.05, the difference between the groups is significant (alpha > 95%))

Group	Ext. rate (mm ³ s ⁻¹)	Nozzle T (°C)	UTS		Strain	
			P -value	Conclusion	P -value	Conclusion
F1–F3	0.4	410	0.852	Not different	0.124	Not different
F1–F3	1.2	410	0.033	Different	0.002	Different
F1–F3	2.0	410	0.278	Not different	0.002	Different
F1–F3	0.4	430	0.486	Not different	0.000	Different
F1–F3	1.2	430	0.001	Different	0.000	Different
F1–F3	2.0	430	0.000	Different	0.000	Different
F1–F3	0.4	450	0.316	Not different	0.033	Different
F1–F3	1.2	450	0.889	Not different	0.012	Different
F1–F3	2.0	450	0.297	Not different	0.026	Different

Table 9 Crystallinity level for F1 extruded filaments determined through XRD measurements

Extrusion rate (mm ³ s ⁻¹)	Nozzle T (°C)					
	410		430		450	
	Crystallinity %	SD	Crystallinity %	SD	Crystallinity %	SD
0.4	12.3	1.3	12.2	0.4	11.8	0.3
1.2	24.2	1.0	23.4	2.0	22.6	0.7
2.0	19.2	0.6	18.7	2.3	16.2	1.3

Table 10 Crystallinity level for extruded F3 filaments determined through XRD measurements

Extrusion rate (mm ³ s ⁻¹)	Nozzle T (°C)					
	410		430		450	
	Crystallinity %	SD	Crystallinity %	SD	Crystallinity %	SD
0.4	29.3	0.5	31.8	0.1	31.0	0.6
1.2	30.6	0.9	29.0	0.6	29.6	1.7
2.0	30.0	1.6	30.1	0.1	29.6	1.2

Figure 18 XRD curves for F1 and F3 after extrusion (@430 °C–4.5 mm³ s⁻¹).

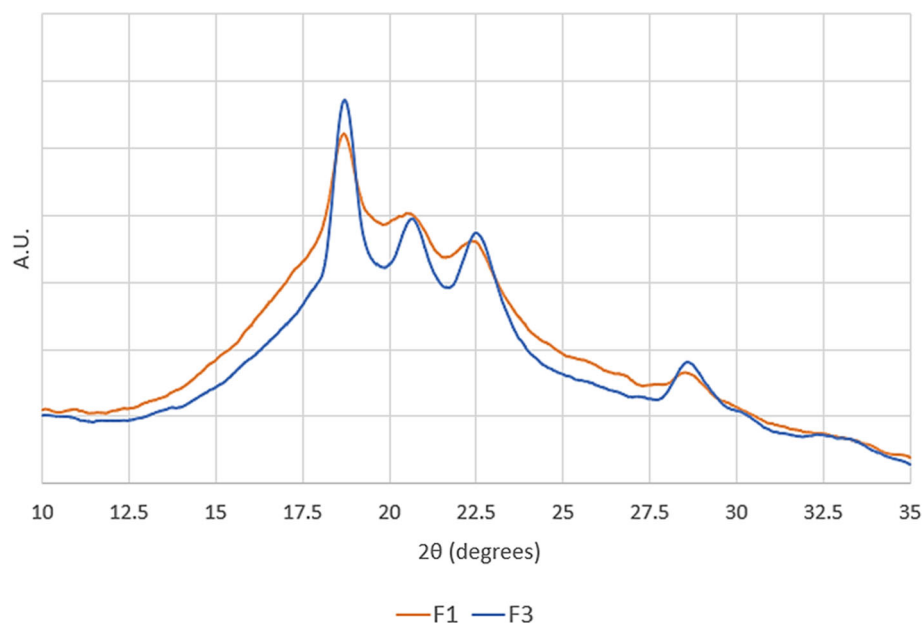


Table 11 Residual crystallinity of feedstock filament F1. Filament followed a mix of temperatures (310–330 °C) and times (0.1–10 s)

Time (s) >	Crystallinity (%)		
	0.1 s	5 s	10 s
Temperature (°C)			
330.0	0.14	0.08	0.14
327.5	1.07	0.85	1.06
325.0	5.63	5.07	5.73
322.5	8.92	9.34	10.76
320.0	12.47	13.68	14.89
317.5	15.13	15.94	17.24
315.0	17.00	18.41	19.65
312.5	18.82	20.08	21.12
310.0	20.50	21.75	23.19
Reference	30.17%		

during subsequent heating. Table 11 shows the residual crystallinity at the range of isothermal temperatures and times tested.

At 330 °C and above, there is no residual crystallinity left in the polymer, independent of the polymer residence time. As the temperature decreases, the level of residual crystallinity increases to approximately 5% at 325 °C. At temperatures below 325 °C, the residence time appears to increase slightly the crystallinity; hence at 310 °C, 0.1 s residence time retains 20% crystallinity which increases to 23% for 10 s residence time. The increase in residual

crystallinity with an increase in residence time could be the result of polymer chains reorganization.

In comparison with the standard feedstock filament, which was repeatedly cycled, the drawn extruded filament could not be exposed to the same set of experiments as it would require a fresh FDSC microchip for each temperature and time. For this reason, the combination of 317.5 °C at 0.1 s was chosen as the temperature and time to be used with the FDSC to check crystallinity without recrystallization. This set of temperature and time maintains 15% residual crystallinity for the F1 feedstock filament. Figure 19 shows the residual crystallinity for extruded F1 compared with the drawn extruded filament, F3.

Some conclusions can be achieved by comparing both residual crystallinities (10% for F1 and 14% for F3) presented in Fig. 19 with the 15% residual crystallinity shown in Table 11, all carried out at 0.1 s residence time and 317.5 °C. First, the results revealed a slightly higher crystallinity in drawn filament when compared with the standard, which may be related to crystal retention during the process [include references]. Second, the relatively lower value of 10% obtained from the direct measurement of the feedstock F1 (as received) is probably related to a different thermal history not precisely replicated by the isothermal crystallization cycle used as reference.

It is also important to mention that the normal FDSC procedure requires a preparation of the sample

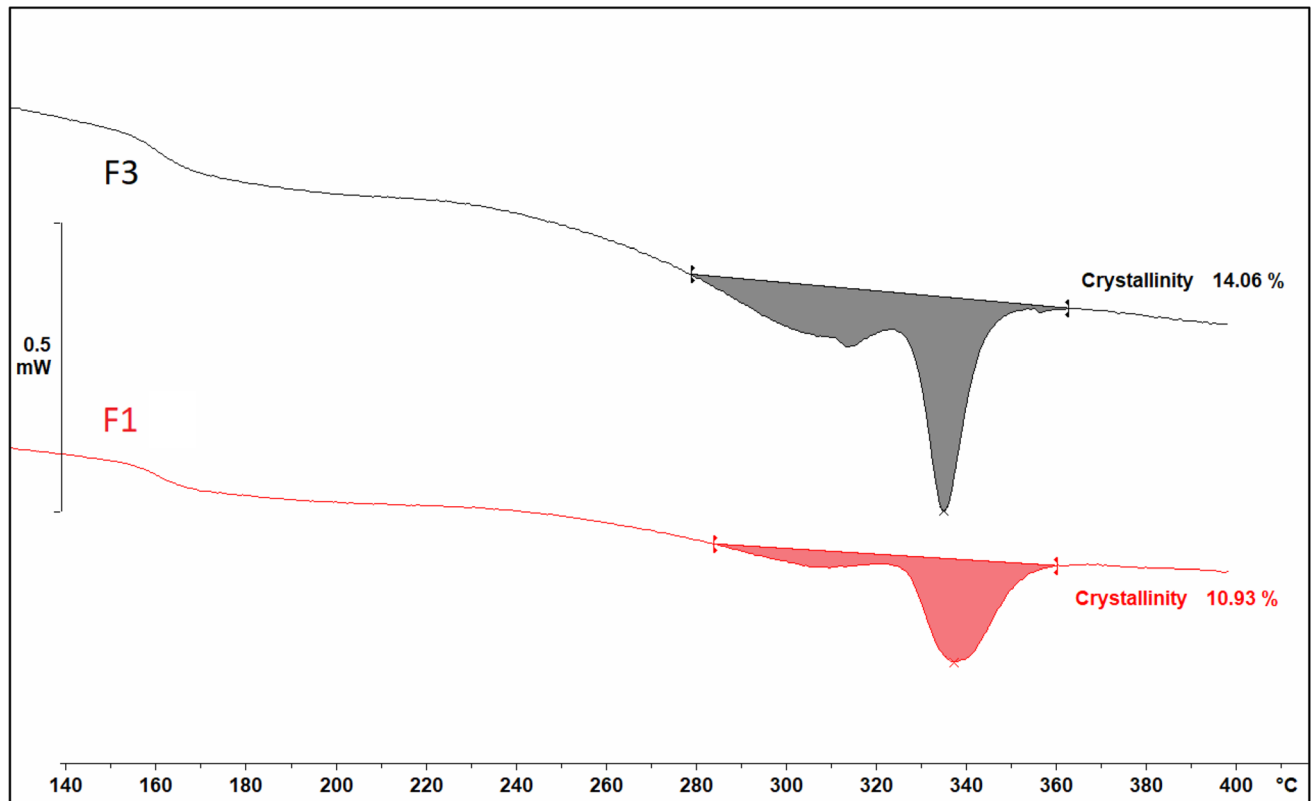


Figure 19 FDSC residual crystallinity for F1 (standard) and F3 (drawn) filament.

on the microchip, using a preheating stage which allows sample to stick to the measuring surface. The lack of sample contact with the microchip can lead to less accurate results and movement of the sample. In this case, the pre-heating of the sample was not possible, as the step would destroy the thermal information required to understand the crystal history of the extruded filaments.

Both DSC traces revealed presence of a double melting peak, which was originally not detected in the feedstock materials using standard DSC (see Figs. 9, 10, 11). The presence of the double melting peak has been argued in the literature. Some authors relate the presence of the double melting peak with double lamellar populations, suggesting the presence of two types of crystals [62, 63], while others also relate the behaviour of the double melting peak with reorganizations of the crystalline structure during the heating of the polymer [50, 61, 64, 65]. According to this approach, the lamellae with a lower melting

point would form last and would be concentrated in the peripheral regions of the crystallites, presenting a reorganization and shifting towards the higher melting peak, especially when using lower heating rates in a DSC analysis. However, by using the high heating rate provided by the FDSC, the double melting peak could be detected as shown in Fig. 19, with the lower temperature melting peak presenting a smaller amplitude when compared to the higher temperature peak. In addition, it is also possible to observe a sharper peak for F3, with a slightly lower melting temperature, similar to the feedstock response, suggesting again some crystalline memory retention.

Conclusions

According to the experimental results, crystallinity levels and polymer structure are affected by the production process of filament shaped polymers. The

drawn PEEK feedstock filament (F3) presented considerable differences in mechanical properties and XRD results, showing a spectra pattern with considerable increase in intensity of the peaks representing the (110) and (200) planes, not observed in the (111) plane, which was mostly hidden.

Since drawn PEEK feedstock was able to provide a higher strength performance (almost 4X higher than traditional feedstocks) as pointed by tensile tests, further tests were conducted to understand if these properties could be transferred to FFF extruded PEEK filaments.

The tensile test showed that the molecular orientation in the drawn filament influenced the crystallinity and mechanical properties of the extruded PEEK filaments. Drawn extruded PEEK filament (F3) presented considerable higher strength and strain values when compared to standard extruded filament (F1). The filaments produced with the drawn feedstock F3, maintained a slightly superior strain performance after extrusion suggesting that the input material affects the results, even after a full melting of the material, as shown by the FDSC results. This result could be related to melt-memory effects that could influence the crystallization of the polymer from the melt [39].

A similar conclusion was obtained from the XRD results on the extruded filaments, with the filaments extruded from the drawn feedstock showing more defined and sharp peaks, associated with greater crystallinity, which was also supported by the FDSC results, with drawn PEEK showing higher values of remaining crystallinity.

By extruding the filament in air, the experiments helped to isolate the extrusion effects before and after the process without the influence of mechanical interaction with the previous layers or substrate temperature helping to understand the dynamics of crystallization under these conditions.

Such conclusions suggest that it is possible to influence the properties of the extruded filaments depending on the specific properties of the feedstock, which could lead, for example, to improvements in the properties of the parts produced. Furthermore, it is important to check the feedstock quality and structure prior to printing if consistent parts are to be achieved.

Open Access This article is licensed under a Creative Commons Attribution 4.0 International License, which permits use, sharing, adaptation, distribution and reproduction in any medium or format, as long as you give appropriate credit to the original author(s) and the source, provide a link to the Creative Commons licence, and indicate if changes were made. The images or other third party material in this article are included in the article's Creative Commons licence, unless indicated otherwise in a credit line to the material. If material is not included in the article's Creative Commons licence and your intended use is not permitted by statutory regulation or exceeds the permitted use, you will need to obtain permission directly from the copyright holder. To view a copy of this licence, visit <http://creativecommons.org/licenses/by/4.0/>.

References

- [1] Popescu D, Zapciu A, Amza C et al (2018) FDM process parameters influence over the mechanical properties of polymer specimens: a review. *Polym Test* 69:157–166. <https://doi.org/10.1016/j.polymertesting.2018.05.020>
- [2] Mohamed OA, Masood SH, Bhowmik JL (2016) Mathematical modeling and FDM process parameters optimization using response surface methodology based on Q-optimal design. *Appl Math Model* 40:10052–10073. <https://doi.org/10.1016/j.apm.2016.06.055>
- [3] Mohamed OA, Masood SH, Bhowmik JL (2017) Process parameter optimization of viscoelastic properties of FDM manufactured parts using response surface methodology. *Mater Today Proc* 4:8250–8259. <https://doi.org/10.1016/j.matpr.2017.07.167>
- [4] Raut S, Jatti VS, Khedkar NK, Singh TP (2014) Investigation of the effect of built orientation on mechanical properties and total cost of FDM parts. *Procedia Mater Sci* 6:1625–1630. <https://doi.org/10.1016/j.mspro.2014.07.146>
- [5] Ceretti E, Ginestra P, Neto PI et al (2017) Multi-layered scaffolds production via Fused Deposition Modeling (FDM) using an open source 3D printer: process parameters optimization for dimensional accuracy and design reproducibility. *Procedia CIRP* 65:13–18. <https://doi.org/10.1016/j.procir.2017.04.042>
- [6] De Ciurana J, Serenó L, Vallès È (2013) Selecting process parameters in RepRap additive manufacturing system for

- PLA scaffolds manufacture. *Procedia CIRP* 5:152–157. <https://doi.org/10.1016/j.procir.2013.01.031>
- [7] Khabia S, Jain KK (2019) Comparison of mechanical properties of components 3D printed from different brand ABS filament on different FDM printers. *Mater Today Proc* 26:2907–2914. <https://doi.org/10.1016/j.matpr.2020.02.600>
- [8] Gebisa AW, Lemu HG (2019) Influence of 3D printing FDM process parameters on tensile property of ULTEM 9085. *Procedia Manuf* 30:331–338. <https://doi.org/10.1016/j.promfg.2019.02.047>
- [9] Bellini A, Gucceri S, Bertoldi M (2004) Liquefier dynamics in fused deposition. *J Manuf Sci Eng* 126:237. <https://doi.org/10.1115/1.1688377>
- [10] Sajan N, John TD, Sivadasan M, Singh NK (2018) An investigation on circularity error of components processed on Fused Deposition Modeling (FDM). *Mater Today Proc* 5:1327–1334. <https://doi.org/10.1016/j.matpr.2017.11.218>
- [11] Yin J, Lu C, Fu J et al (2018) Interfacial bonding during multi-material fused deposition modeling (FDM) process due to inter-molecular diffusion. *Mater Des* 150:104–112. <https://doi.org/10.1016/j.matdes.2018.04.029>
- [12] Mishra SB, Abhishek K, Satapathy MP, Mahapatra SS (2017) Parametric appraisal of compressive strength of FDM build parts. *Mater Today Proc* 4:9456–9460. <https://doi.org/10.1016/j.matpr.2017.06.203>
- [13] Mohan N, Senthil P, Vinodh S, Jayanth N (2017) A review on composite materials and process parameters optimisation for the fused deposition modelling process. *Virtual Phys Prototyp* 12:47–59. <https://doi.org/10.1080/17452759.2016.1274490>
- [14] Cain P (2019) Selecting the optimal shell and infill parameters for FDM 3D Printing. <https://www.3dhubs.com/knowledge-base/selecting-optimal-shell-and-infill-parameters-fdm-3d-printing>. Accessed 10 Feb 2019
- [15] Cain P (2019) The impact of layer height on a 3D Print. <https://www.3dhubs.com/knowledge-base/impact-layer-height-3d-print>. Accessed 13 February 2019
- [16] Tran N, Nguyen V, Ngo A, Nguyen V (2017) Study on the effect of fused deposition modeling (FDM) process parameters on the printed part quality. *Int J Eng Res Appl* 7:71–77. <https://doi.org/10.9790/9622-0712027177>
- [17] El Magri A, El Mabrouk K, Vaudreuil S et al (2020) Optimization of printing parameters for improvement of mechanical and thermal performances of 3D printed poly(ether ether ketone) parts. *J Appl Polym Sci* 137:1–14. <https://doi.org/10.1002/app.49087>
- [18] El Magri A, Vanaei S, Vaudreuil S (2021) An overview on the influence of process parameters through the characteristic of 3D-printed PEEK and PEI parts. *High Perform Polym*. <https://doi.org/10.1177/09540083211009961>
- [19] Wittbrodt B, Pearce JM (2015) The effects of PLA color on material properties of 3-D printed components. *Addit Manuf* 8:110–116. <https://doi.org/10.1016/j.addma.2015.09.006>
- [20] Pires FQ, Alves-Silva I, Pinho LAG et al (2020) Predictive models of FDM 3D printing using experimental design based on pharmaceutical requirements for tablet production. *Int J Pharm* 588:119728. <https://doi.org/10.1016/j.ijpharm.2020.119728>
- [21] Srinivasan R, Pridhar T, Ramprasath LS et al (2020) Prediction of tensile strength in FDM printed ABS parts using response surface methodology (RSM). *Mater Today Proc* 27:1827–1832. <https://doi.org/10.1016/j.matpr.2020.03.788>
- [22] de León AS, Domínguez-Calvo A, Molina SI (2019) Materials with enhanced adhesive properties based on acrylonitrile-butadiene-styrene (ABS)/thermoplastic polyurethane (TPU) blends for fused filament fabrication (FFF). *Mater Des* 182:108044. <https://doi.org/10.1016/j.matdes.2019.108044>
- [23] Khan MS, Mishra SB (2019) Minimizing surface roughness of ABS-FDM build parts: an experimental approach. *Mater Today Proc* 26:1557–1566. <https://doi.org/10.1016/j.matpr.2020.02.320>
- [24] Corapi D, Morettini G, Pascoletti G, Zitelli C (2019) Characterization of a polylactic acid (PLA) produced by Fused Deposition Modeling (FDM) technology. *Procedia Struct Integr* 24:289–295. <https://doi.org/10.1016/j.prostr.2020.02.026>
- [25] Geng P, Zhao J, Wu W et al (2019) Effects of extrusion speed and printing speed on the 3D printing stability of extruded PEEK filament. *J Manuf Process* 37:266–273. <https://doi.org/10.1016/j.jmapro.2018.11.023>
- [26] 3D Matter (2019) FDM 3D Printing materials compared. <https://www.3dhubs.com/knowledge-base/fdm-3d-printing-materials-compared>. Accessed 17 Jun 2019
- [27] Azimi P, Zhao D, Pouzet C et al (2016) Emissions of ultrafine particles and volatile organic compounds from commercially available desktop three-dimensional printers with multiple filaments. *Environ Sci Technol* 50:1260–1268. <https://doi.org/10.1021/acs.est.5b04983>
- [28] Kumar MA, Khan MS, Mishra SB (2020) Effect of machine parameters on strength and hardness of FDM printed carbon fiber reinforced PETG thermoplastics. *Mater Today Proc* 27:975–983. <https://doi.org/10.1016/j.matpr.2020.01.291>
- [29] Sathish Kumar K, Soundararajan R, Shanthosh G et al (2020) Augmenting effect of infill density and annealing on mechanical properties of PETG and CFPETG composites fabricated by FDM. *Mater Today Proc*, pp 2–7. <https://doi.org/10.1016/j.matpr.2020.10.078>
- [30] Ramesh M, Panneerselvam K (2020) Mechanical investigation and optimization of parameter selection for Nylon

- material processed by FDM. *Mater Today Proc.* <https://doi.org/10.1016/j.matpr.2020.02.697>
- [31] Wang S, Ma Y, Deng Z et al (2020) Effects of fused deposition modeling process parameters on tensile, dynamic mechanical properties of 3D printed polylactic acid materials. *Polym Test* 86:106483. <https://doi.org/10.1016/j.polymertesting.2020.106483>
- [32] Puigoriol-Forcada JM, Alsina A, Salazar-Martín AG et al (2018) Flexural fatigue properties of polycarbonate fused-deposition modelling specimens. *Mater Des* 155:414–421. <https://doi.org/10.1016/j.matdes.2018.06.018>
- [33] Rinaldi M, Ghidini T, Cecchini F et al (2018) Additive layer manufacturing of poly (ether ether ketone) via FDM. *Compos Part B Eng* 145:162–172. <https://doi.org/10.1016/j.compositesb.2018.03.029>
- [34] Tseng JW, Liu CY, Yen YK et al (2018) Screw extrusion-based additive manufacturing of PEEK. *Mater Des* 140:209–221. <https://doi.org/10.1016/j.matdes.2017.11.032>
- [35] DI Stepashkin C, Senatov FS et al (2018) 3D-printed PEEK-carbon fiber (CF) composites: structure and thermal properties. *Compos Sci Technol* 164:319–326. <https://doi.org/10.1016/j.compscitech.2018.05.032>
- [36] Arif MF, Kumar S, Varadarajan KM, Cantwell WJ (2018) Performance of biocompatible PEEK processed by fused deposition additive manufacturing. *Mater Des* 146:249–259. <https://doi.org/10.1016/j.matdes.2018.03.015>
- [37] Berretta S (2015) Poly Ether Ether Ketone (PEEK) polymers for High Temperature Laser Sintering (HT-LS) Doctoral. University of Exeter
- [38] Doumeng M, Ferry F, Delbe K et al (2019) Evolution of crystallinity of PEEK and glass fibre reinforced PEEK under tribological conditions using Raman spectroscopy. *Wear* 426–427:1040–1046. <https://doi.org/10.1016/j.wear.2018.12.078>
- [39] Muthukumar M (2016) Communication: theory of melt-memory in polymer crystallization. *J Chem Phys* 145. <https://doi.org/10.1063/1.4959583>
- [40] Mamun A, Umamoto S, Okui N, Ishihara N (2007) Self-seeding effect on primary nucleation of isotactic polystyrene. *Macromolecules* 40:6296–6303. <https://doi.org/10.1021/ma070963j>
- [41] Supaphol P, Spruiell JE (2000) Crystalline memory effects in isothermal crystallization of syndiotactic polypropylene. *J Appl Polym Sci* 75:337–346. [https://doi.org/10.1002/\(SICI\)1097-4628\(200011\)75:3%3c337::AID-APP1%3e3.0.CO;2-4](https://doi.org/10.1002/(SICI)1097-4628(200011)75:3%3c337::AID-APP1%3e3.0.CO;2-4)
- [42] Erukhimovich I, de la Cruz MO (2004) Phase equilibria and charge fractionation in polydisperse polyelectrolyte solutions. *J Polymer Sci*, pp 1738–1750. <https://doi.org/10.1002/polb.21300>
- [43] Tlegenov Y, Wong YS, Hong GS (2017) A dynamic model for nozzle clog monitoring in fused deposition modelling. *Rapid Prototyp J* 23:391–400. <https://doi.org/10.1108/RPJ-04-2016-0054>
- [44] Srivastava M, Maheshwari S, Kundra TK (2015) Virtual modelling and simulation of functionally graded material component using FDM technique. *Mater Today Proc* 2:3471–3480. <https://doi.org/10.1016/j.matpr.2015.07.323>
- [45] Victrex (2019) Victrex PEEK 450g
- [46] Wang P, Zou B, Xiao H et al (2019) Effects of printing parameters of fused deposition modeling on mechanical properties, surface quality, and microstructure of PEEK. *J Mater Process Tech* 271:62–74. <https://doi.org/10.1016/j.jmatprotec.2019.03.016>
- [47] Duddleston LJJ, Woznick K, Koch C, et al (2017) Extrudate mass flow rate analysis in Fused Filament Fabrication (FFF): a cursory investigation of the effects of printer parameters. In: *Annu Tech Conf—NTEC, Conf Proc 2017-May*, pp 43–48
- [48] Blundell DJ, Osborn BN (1983) The morphology of poly(aryl-ether-ether-ketone). *Polymer (Guildf)* 24:953–958. [https://doi.org/10.1016/0032-3861\(83\)90144-1](https://doi.org/10.1016/0032-3861(83)90144-1)
- [49] Sun Q, Rizvi GM, Bellehumeur CT, Gu P (2008) Effect of processing conditions on the bonding quality of FDM polymer filaments. *Rapid Prototyp J* 14:72–80. <https://doi.org/10.1108/13552540810862028>
- [50] Tardif X, Pignon B, Boyard N et al (2014) Experimental study of crystallization of PolyEtherEtherKetone (PEEK) over a large temperature range using a nano-calorimeter. *Polym Test* 36:10–19. <https://doi.org/10.1016/j.polymertesting.2014.03.013>
- [51] Wang Y, Chen B, Evans K, Ghita O (2018) Enhanced ductility of PEEK thin film with self assembled fibre like crystals. *Sci Rep* 8:1314. <https://doi.org/10.1038/s41598-018-19537-1>
- [52] Wang Y, Chen B, Evans KE et al (2016) Novel fibre-like crystals in thin films of Poly Ether Ether Ketone (PEEK). *Mater Lett* 184:112–118. <https://doi.org/10.1016/j.matlet.2016.08.024>
- [53] Ashby MF, Jones DRH (1991) *Jones Materiaux: 2. microstructures et mise en oeuvre*, Dunod
- [54] Northolt MG, Decker P den, Picken SJ, et al (2005) The tensile strength of polymer fibres fibre modulus. In: *Advances in Polymer Science book series (POLYMER, volume 178)*, pp 1–108
- [55] Gupta VB (1991) Nature of crystals and their influence on fibre properties. *Indian J Fibre Text Res* 16:100–115
- [56] Nogales A, Ezquerro TA, Denchev Z, Baltá-Calleja FJ (2001) Induction time for cold crystallization in semi-rigid

- polymers: PEN and PEEK. *Polymer (Guildf)* 42:5711–5715. [https://doi.org/10.1016/S0032-3861\(00\)00929-0](https://doi.org/10.1016/S0032-3861(00)00929-0)
- [57] Liu T, Mo Z, Wang S, Zhang H (1997) Nonisothermal melt and cold crystallization kinetics of poly(aryl ether ether ketone ketone). *Polym Eng Sci* 37:568–575. <https://doi.org/10.1002/pen.11700>
- [58] Kadiyala AK, Bijwe J, Kalappa P (2018) Investigations on influence of nano and micron sized particles of SiC on performance properties of PEEK coatings. *Surf Coatings Technol* 334:124–133. <https://doi.org/10.1016/j.surfcoat.2017.11.026>
- [59] Doumeng M, Makhlof L, Berthet F et al (2021) A comparative study of the crystallinity of polyetheretherketone by using density, DSC, XRD, and Raman spectroscopy techniques. *Polym Test*, 93. <https://doi.org/10.1016/j.polymertesting.2020.106878>
- [60] Karacan I (2015) X-ray Diffraction Studies of Poly (aryl ether ether ketone) Fibers with different degrees of crystallinity and orientation. *Fibers Polym* 6:206–2018. <https://doi.org/10.1007/BF02875644>
- [61] Blundell DJ (1987) On the interpretation of multiple melting peaks in poly(ether ether ketone). *Polymer (Guildf)* 28:2248–2251. [https://doi.org/10.1016/0032-3861\(87\)90382-X](https://doi.org/10.1016/0032-3861(87)90382-X)
- [62] Cebe P (1988) Application of the Parallel Avrami Model to Crystallization of Poly(Etheretherketone). 28
- [63] Bassett DC, Olley RH, Al Raheil IAM (1988) On crystallization phenomena in PEEK. *Polymer (Guildf)* 29:1745–1754. [https://doi.org/10.1016/0032-3861\(88\)90386-2](https://doi.org/10.1016/0032-3861(88)90386-2)
- [64] Cheng SZD, Cao MY, Wunderlich B (1986) Glass transition and melting behavior of Poly(oxy-1,4-phenyleneoxy-1,4-phenylenecarbonyl-1,4-phenylene). *Macromolecules* 19:1868–1876. <https://doi.org/10.1021/ma00181a040>
- [65] Lee Y, Lin JS (1989) On the Double-melting behavior of poly (ether ether ketone). *Macromolecules* 1760:1756–1760

Publisher's Note Springer Nature remains neutral with regard to jurisdictional claims in published maps and institutional affiliations.